AGU ADVANCING EARTH AND SPACE SCIENCES

Geophysical Research Letters®

RESEARCH LETTER
10.1029/2026GL123203

Capturing the Global Variability of Marine Particulate Organic Carbon Flux: A Hierarchical Bayesian Approach

P. Edwards[1,2], G. L. Britten[3], L. Biermann[4], L. Guidi[5], S. A. Henson[1,2], C. M. Moore[2], S. Ramondenc[5], and B. B. Cael[1,6]

[1]NOC—National Oceanography Centre, Southampton, UK, [2]University of Southampton, Southampton, UK, [3]Biology Department, Woods Hole Oceanographic Institution, Woods Hole, MA, USA, [4]EUMETSAT—European Organisation for the Exploitation of Meteorological Satellites, Darmstadt, Germany, [5]Laboratoire d'Océanographie de Villefranche, Sorbonne University, Villefranche-sur-Mer, France, [6]Department of the Geophysical Sciences, University of Chicago, Chicago, IL, USA

Key Points:

- Our method allows for the separate quantification of the mean POC flux and the contribution from episodic pulses
- The global total POC flux is 6.1 ± 0.17 GtC yr^{-1} at 100 m, 52% of which is due to episodic POC flux pulses
- Flux attenuation is higher toward the equator and lower toward the poles, but with higher variability in attenuation in polar regions

Supporting Information:

Supporting Information may be found in the online version of this article.

Correspondence to:

P. Edwards,
p.edwards@soton.ac.uk

Citation:

Edwards, P., Britten, G. L., Biermann, L., Guidi, L., Henson, S. A., Moore, C. M., et al. (2026). Capturing the global variability of marine particulate organic carbon flux: A hierarchical Bayesian approach. *Geophysical Research Letters*, *53*, e2026GL123203. https://doi.org/10.1029/2026GL123203

Received 23 MAR 2026
Accepted 7 JUL 2026

Abstract Particulate organic carbon (POC) fluxes are important for the marine carbon cycle; however, these fluxes are highly variable in both space and time. Consequently, current estimates retain high uncertainty when predicting POC flux from environmental drivers because the influence of pulse events is not adequately accounted for. Here, by using a hierarchical Bayesian regression model, we explicitly and simultaneously model the mean and variance of POC flux as a function of environmental variables. Our model reproduces the observed distribution of POC fluxes by accounting for flux variance, and estimates global POC flux at ~6 GtC yr^{-1} at 100 m, of which 52% is due to the influence of episodic pulse events. Additionally, spatial patterns in vertical attenuation rates and its stochasticity can be estimated. Therefore, quantifying the small-scale variability introduced through pulse events may be equally as important as understanding specific export pathways.

Plain Language Summary The sinking of organic particles from the surface ocean can sequester carbon in the deep ocean for tens to thousands of years. The amount of carbon stored, however, varies greatly across current estimates due to differences in the techniques used to determine the carbon fluxes and the uncertainty in the data itself. Carbon flux measurements are known to be highly variable in time and space which makes it very difficult to accurately model flux at the global scale. In addition, episodic high-intensity flux events may have important impacts that are not always captured in global estimates. Here we use a mathematical approach that allows for variability, including pulse events. This captured the spread of the data significantly better than approaches that ignore variability. We also find that the estimated global flux of organic carbon sinking out of the surface ocean is higher when variability is included. This shows how important pulse events are in the flux of carbon to the ocean interior and the seafloor.

1. Introduction

The Biological Carbon Pump (BCP) describes a set of biological processes through which CO_2 is converted into organic matter by phytoplankton, a fraction of which sinks into the ocean interior and is remineralized into dissolved inorganic carbon (DIC) (Volk & Hoffert, 1985). The magnitude of the BCP is described by the flux of particulate organic carbon (POC) out of the upper ocean and its subsequent remineralization at depth (Doney et al., 2024; Siegel et al., 2023). Carbon exported via the BCP can remain stored for centuries to millennia when remineralized in the deep ocean (> 1000 m) (Iversen, 2023). This process is fundamental to the functioning of the global carbon cycle by maintaining the deep DIC reservoir, and fueling the mesopelagic and benthic communities (Iversen, 2023).

The magnitude of POC flux is highly variable as a result of several processes driving the initial POC formation and consequent remineralization. This includes phytoplankton community composition, the sinking speeds of marine particles, diurnally vertically migrating (DVM) species, and oceanic currents for example, all of which, in turn, are affected by additional environmental factors (Boyd et al., 2019; Bristow et al., 2017; Lévy et al., 2013; Resplandy et al., 2019; Trudnowska et al., 2021). The variability of these processes leads to pulsed episodicity in POC fluxes, where stochastic periods of high export occur in addition to the background level of flux (Smith et al., 2018).

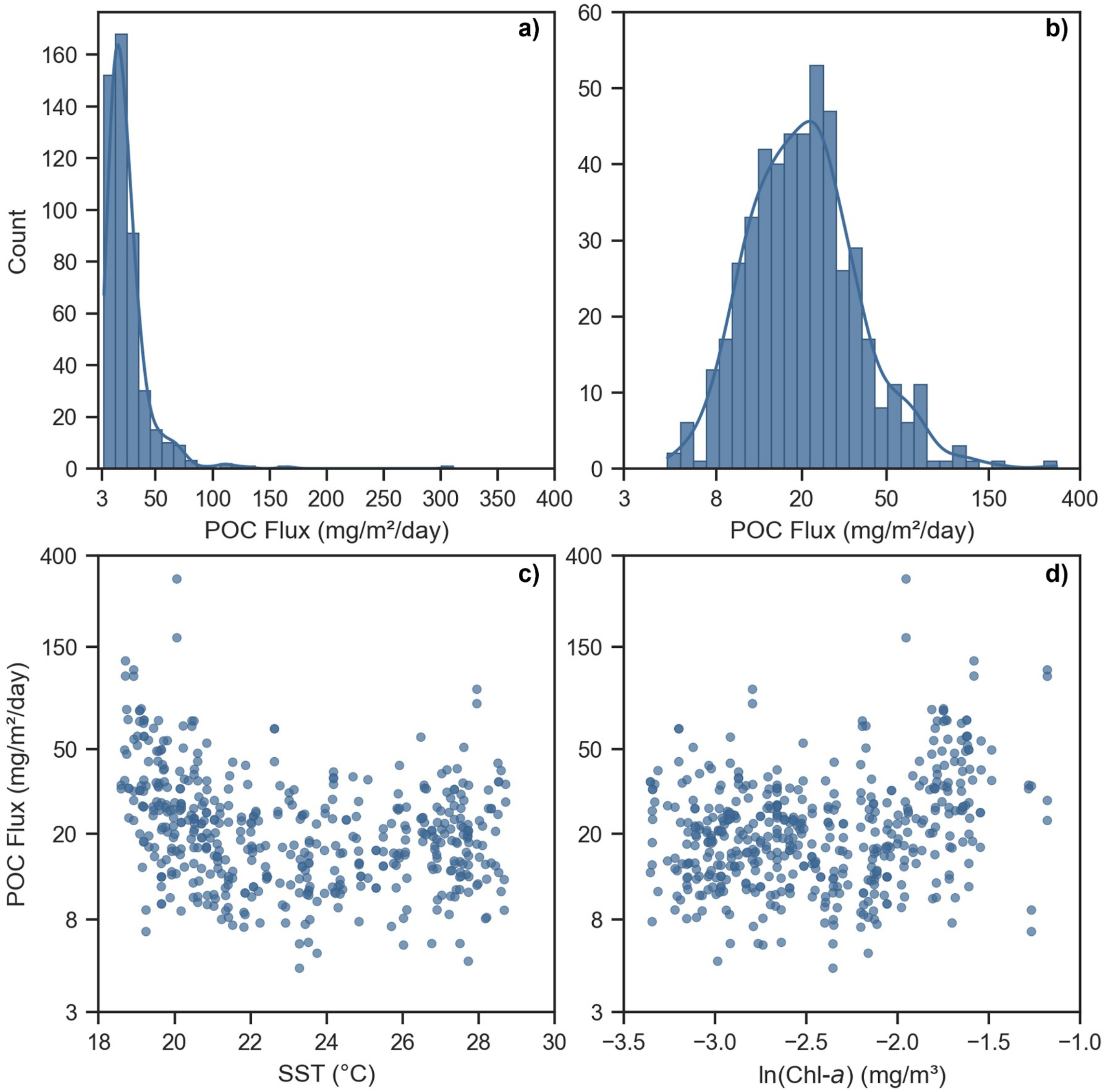

Figure 1. Example of POC flux data distribution at the Bermuda Atlantic Time-series Study (BATS) site (Latitude ~31°, Longitude ~−64°), based on almost 500 measurements collected at 200 m depth from 1997 to 2017. Panels (a) and (b) show the log-normality of the data distribution of POC flux on (a) linear and (b) natural log scale. Panels (c) and (d) show the relationship between SST and Chl-*a* with ln(POC Flux) respectively.

The influence that pulse events have on POC flux causes a heavy positive-skew (or right-tail) to the overall global distribution. This can be represented as a log-normal distribution, which has previously been well described on a global scale (Cael et al., 2018, 2021) and is visible, for example, at the Bermuda Atlantic Time-series Study (BATS) site at 200 m depth for the period 1997–2017 (Figures 1a and 1b). The presence of pulse events increases the mean POC flux value, such that the mean will be higher than the median and dependent on the (log-)variance of the data. In the case of the BATS example, the mean POC flux at 200 m depth is 25.1 mg m^{-2} day^{-1}, whereas the median is 20.2 mg m^{-2} day^{-1}. It is also hard to correlate POC flux and pulse events to specific drivers (Smith et al., 2018) (Figures 1c and 1d). As a result, not capturing the variance and therefore pulse events in global POC flux estimates could result in an underestimation of the total flux.

The current estimates of global POC flux are varied, with the majority of the gravitational sinking flux estimates of POC ranging between 4 and 12 GtC yr^{-1} (Boyd et al., 2019; Clements et al., 2023). Estimates within the lower range of globally integrated values tend to be "bottom-up," where empirical relationships between a compilation of POC flux estimates and predictor variables, such as Sea Surface Temperature (SST) and Net Primary

Production (NPP), are used to scale to global estimates (e.g., Clements et al., 2023; Henson et al., 2011; Siegel et al., 2014). "Top-down" models are based on large scale inversions of remineralization tracers (e.g., oxygen or nutrients) and tend toward higher globally integrated POC flux estimates at the base of the euphotic zone (e.g., DeVries & Weber, 2017; Nowicki et al., 2022; Wang et al., 2023). Though there are several differences between the top-down and bottom-up approaches, a potentially important factor contributing to the differences in global export estimates is that top-down approaches implicitly include pulse events, provided they leave an imprint in the tracer fields, whereas current bottom-up approaches minimize the effect of outliers when constructing the empirical relationships. As such, bottom-up estimates might underestimate global export unless variance is accounted for.

The efficiency of the BCP is described by the rate of remineralization of POC with depth, which is commonly assumed to follow a power law such as the Martin's curve, where POC flux at a given depth z can be described as $F_z = F_{ref}\left(\frac{Z}{Z_{ref}}\right)^b$, where F_{ref} is the flux at a reference depth Z_{ref} (Martin et al., 1987). The parameter b represents the attenuation rate of POC flux, with larger b suggesting a higher rate of attenuation. Spatial patterns in b may be driven by factors such as temperature, plankton and microbial community composition (Bressac et al., 2024, and references therein). However, previous literature is not consistent in describing global-scale spatial patterns, with some studies suggesting low b at the equator and high b at high latitudes (e.g., Guidi et al., 2015; Henson et al., 2012), and others suggesting the opposite (e.g., DeVries & Weber, 2017; Marsay et al., 2015; Weber et al., 2016).

We hypothesize that using a bottom-up statistical model which explicitly accounts for pulse events through modeling the variance and median simultaneously in the data will better capture the relationship between POC flux, attenuation and their drivers. By including multiplicative interactions within this model we also map the spatial distribution of Martin's b parameter. We adopt a Bayesian approach which allows for a rigorous treatment of model uncertainty while incorporating flexible constraints regarding the allowable range of model parameters (Britten et al., 2021; Lambert, 2018). We map the log-variance and log-mean POC flux on a global scale with three predictor variables: satellite derived chlorophyll-*a* (Chl-*a*) concentration, SST, and the depth of measurement. Using this method the strength of each drivers' influence on POC flux, attenuation and variance is quantified and a globally integrated estimate is formed.

2. Methods

2.1. Data Selection

A comprehensive database of in situ POC flux measurements was compiled within Ramondenc et al. (2026). The data set consists of almost 34,000 oceanic POC flux observations which have a date, depth and position at high spatio-temporal coverage from various collection methods (Figure S1; Table S1 in Supporting Information S1). Flux measurements for match-ups were considered from all methods because some important productive regions were not sampled by sediment traps, making the full database more globally representative (Figure S1 in Supporting Information S1). This choice may introduce some measurement bias into our estimates, but this bias cannot be quantified from the available data and is probably small compared to the bias that would result from using a less globally representative data set. Measurements were not considered if they were collected at depths shallower than 100 m or if the flux fell below 0.1mgC m^{-2} day^{-1} so that measurement error is not dominating the flux value (Cael et al., 2018). Note this is considerably smaller than the cut-off 3.6 mgC m^{-2} day^{-1} used in Cael et al. (2018).

For each POC flux data point, corresponding SST and Chl-*a* measurements were selected from monthly mean satellite derived data sets in the year range of 1997–2022. SST (°C) was obtained from the Merged Hadley-NOAA/OI Sea Surface Temperature data set at 1° resolution (Hurrell et al., 2008; Shea et al., 2024). Chla-*a* concentrations were obtained from the Ocean Colour Climate Change Initiative (OC-CCI) version 6.0, re-gridded from 4 km to 1° resolution and converted into μg m^{-3} (Sathyendranath et al., 2019, 2023). Not all POC flux data had matching SST or Chl-*a* data due to cloud cover, polar night, or being outside the temporal range of the satellite time-series, and were hence discarded. Data points were also excluded if under ice or if Chl-*a* concentrations were smaller than 20 μg m^{-3} to remove the influence of very small values on the log-normal distribution. This left 12,936 data points for analysis across all ocean basins with a range of coastal, open ocean, singular and temporally repeated locations, of which 94% were from sediment traps (Figure S1; Table S1 in Supporting Information S1). Re-running the data analysis without non-sediment trap data does not cause major changes in the posterior coefficients, but means that there is less range in predictors and spatiotemporal variability (Table S2 in Supporting Information S1).

The use of other potential drivers (or correlates of drivers) was considered, including distributions of nitrate, phosphate and silicate concentrations from the World Ocean Atlas 2023 data set (Garcia et al., 2024). However, as these are only available as climatologies, they do not have the same temporal and spatial coverage as the other potential drivers, thus severely limiting the size and event-scale statistical properties of the available data and, when included, made no overall improvement to the model (Table S3 in Supporting Information S1).

2.2. Hierarchical Model

A Bayesian hierarchical approach allows for the mean and variance of the log-transformed POC flux distribution to be modeled simultaneously. All predictors were log-transformed before use in the model, with 1.79°C added to SST to ensure positive values before log-transformation. Both the mean and variance of ln(POC flux) are explicitly modeled as a function of the predictor variables: Z, ln(measurement depth); T, ln(SST + 1.79); C, ln(chl - a); and their interactions (TC, TZ and CZ).

Following previous studies, we first assumed that individual log-transformed observations followed a normal distribution of the form:

$$y_i \sim \mathcal{N}(\mu_i, \sigma_i) \tag{1}$$

where y_i is an observation of ln(POC flux) described by a normal distribution with a median of μ_i and standard deviation of σ_i. The i subscript indicates that each flux measurement will have its own predicted mean and variance (of the distribution it is drawn from), according to the values of the predictor variables. The relationships between μ_i, σ_i and the predictor variables were captured using the following linear relationships:

$$\mu_i = \beta_0 + \beta_{T0} T_i + (\beta_{C0} + \beta_{CT} T_i) C_i + (\beta_{Z0} + \beta_{TZ} T_i + \beta_{CZ} C_i) Z_i \tag{2}$$

$$\sigma_i = \gamma_0 + \gamma_{T0} T_i + (\gamma_{C0} + \gamma_{CT} T_i) C_i + (\gamma_{Z0} + \gamma_{TZ} T_i + \gamma_{CZ} C_i) Z_i \tag{3}$$

where β_0 represents the intercept for the μ relationship, while β_{T0}, β_{C0}, β_{Z0}, β_{TC}, β_{TZ} and β_{CZ} represent the slopes on T, C, Z and interactions TC, TZ and CZ respectively. Coefficients for σ are defined analogously. A prior assumption is set on σ to ensure it is positive; no other prior constraints were set.

In summary, this model allows for the predictor variables of depth, Chl-a and SST to have unique effects on the median and standard deviation of the observed ln(POC flux) flux. The coefficients for the predictors were calculated through linear regression within the Hierarchical Bayesian model using a Markov Chain Monte Carlo (MCMC), with all chains converging (Figure S2 in Supporting Information S1). All $\hat{R}$ scores for each predictor were between 0.99 and 1.01 (Gelman & Rubin, 1992). The hierarchical component allows us to simultaneously model a linear log-median relationship (μ) between log-transformed predictors and ln(POC flux), and linear form between the standard deviation (σ) and the log-transformed predictors. The model was developed and fit using the Stan probabilistic programming language and its Python-based wrapper CmdStanPy 1.2.5 (Carpenter et al., 2017).

2.3. Posterior Analysis

To test if the model was able to capture the observed distribution of POC flux, the generated values of μ and σ were used to create two data sets from the predictor variables (so-called posterior predictive distributions). For each observation of POC flux, a random data point y_{sim} was drawn from the generated normal distribution such that:

$$\ln(y_{\text{sim}}) \sim \mathcal{N}(\mu_i, \sigma_i) \tag{4}$$

10.1029/2026GL123203

This was repeated with

$$\ln\left(y_{\mathrm{sim0}}\right) \sim \mathcal{N}\left(\mu_i, 0\right) \tag{5}$$

where y_{sim0} represents a sample from a posterior predictive distribution where the influence from variance and pulse events is ignored. The mean μ_i and σ_i for each data point from the MCMC output were used in these equations. Kolmogorov-Smirnov (K-S) statistics are used to compare the original and recreated distribution of POC flux, indicating goodness of fit at the distribution level. Pearson correlation coefficients (r) and r^2 values were also calculated for the comparison between observed and synthetic data sets.

For further validation analysis, 10 random subsets, split into 90% training data and 10% test data were chosen to test the predictive capacity of the model. These performed similarly to the model built on the whole data set (Figure S3, Table S4 in Supporting Information S1). In all cases, the K-S statistics with σ indicated a better goodness-of-fit despite lower overall r. This is because explicitly accounting for σ does not provide predictive power, but rather improves the statistical characterization of residuals.

2.4. Global Distributions

To calculate global monthly mean POC flux at 100 m depth, the derived relationships for μ, σ and the mean POC flux were applied to a $1 \times 1°$ grid of monthly mean SST and Chl-*a* (over 1997–2022). Assuming log-normal distribution, mean POC flux is calculated as:

$$\text{Mean POC flux} = \mu + \frac{\sigma^2}{2} \tag{6}$$

The mean POC flux for each month, multiplied by the grid cell area, was then summed to calculate the globally integrated annual estimate for POC flux when episodic pulse events are considered. The same approach is applied to μ to provide an estimate of "background flux."

Attenuation is mapped globally using the cross terms related to depth as follows:

$$\beta_Z = \beta_{Z0} + \beta_{TZ}T + \beta_{TC}C \tag{7}$$

where β_Z represents the change in μ, the *median* POC flux, with respect to depth. This relationship can also be applied to calculate the global distribution of γ_Z, the attenuation with depth of *variability* in POC fluxes, using γ_{Z0}, γ_{TZ} and γ_{CZ}. Similar relationships can be applied between other terms for the summative effect sizes of β_T, β_C, γ_T and γ_C.

To estimate the attenuation rate of POC flux with depth, Martin's b, *mean* POC flux was calculated at depths from 100 to 1,500 m in 100 m increments using the global and monthly climatologies of SST and Chl-*a*. These values were then regressed against ln(depth) with the slope of this regression used as a per pixel estimate of attenuation rate such that

$$b = \frac{\delta \ln(\text{POC flux})}{\delta Z} \tag{8}$$

The code for the Hierarchical model and analyses is published on GitHub and can be found at https://github.com/pip-edwards/estpocbayes.

3. Results and Discussion

3.1. Model Performance

We find that our model reproduces the distribution of the POC flux observations (K-S statistic = 0.044, Figure 2a, Figure S4 in Supporting Information S1). In contrast, if σ is ignored within our model $\left(y_{\mathrm{sim0}}\right)$, it does a poor job in reproducing the observed POC flux distribution (K-S statistic = 0.12, Figure 2b, Figure S4 in Supporting

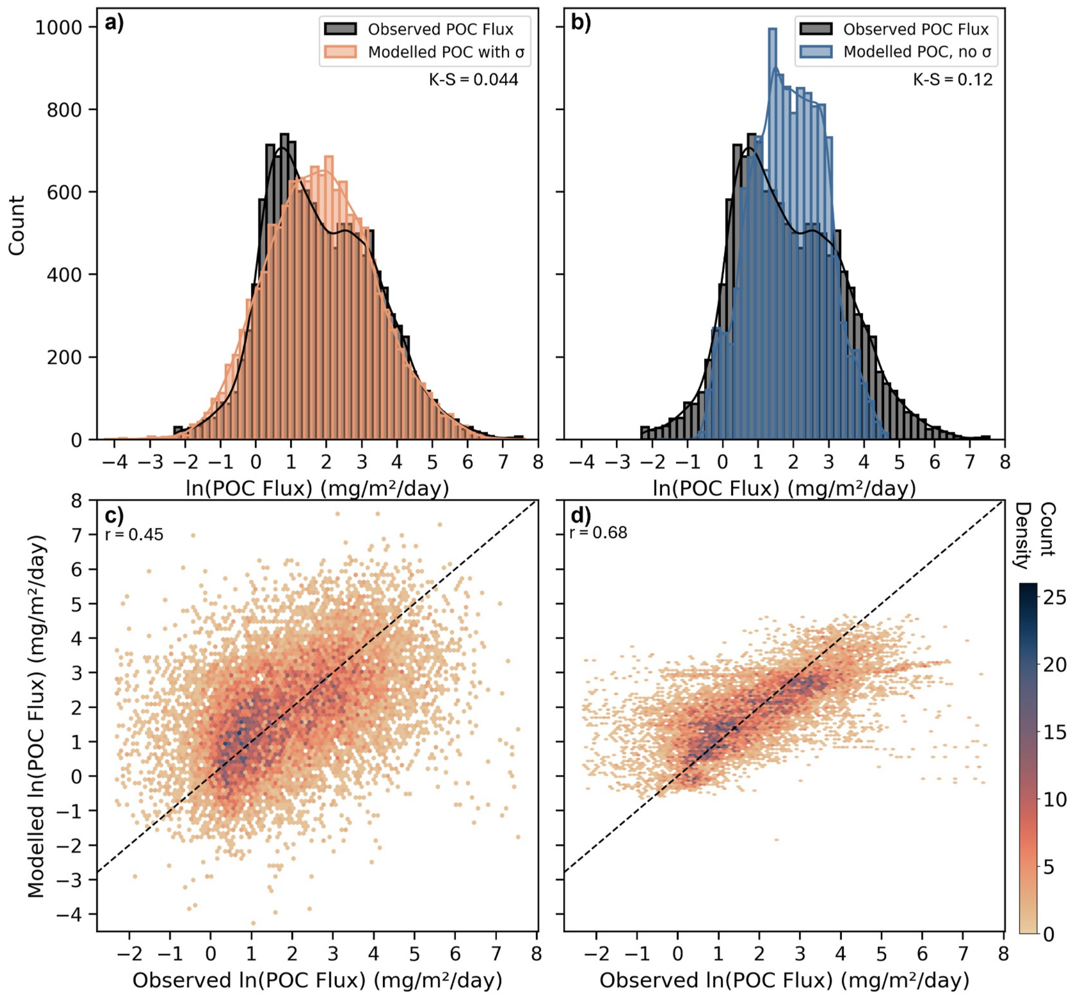

Figure 2. Distribution of model generated POC flux values against observed POC flux shown as histograms (a, b) and scatter plots (c, d). In the scatter plots, the density (number of observations) is indicated by a heat map and the dashed line represents the 1:1 relationship. Panels (a) and (c) show the relationship between the observed data when σ is included in the model while panels (b) and (d) show the relationship between the observed data when $\sigma = 0$ in the model.

Information S1). Without the episodicity accounted for, the model cannot reproduce the upper tail, therefore higher POC flux, of the observed distribution.

When σ is not used to model the data, there is a stronger relationship between the modeled and original POC flux data ($r = 0.45$ with σ and $r = 0.68$ without; both have p values ≈ 0) (Figures 2c and 2d). This is necessarily the case because the inclusion of σ in the model acts as an addition of random noise to the relationship shown in Figure 2d. The model without σ has an r^2 value of 0.45, similar to previous bottom-up models, but with a poorer match to the distribution of the data than our model when including σ (Clements et al., 2023; Dunne et al., 2007; Henson et al., 2011; Siegel et al., 2014) (Figures 2a–2c). Note that the model with σ cannot be compared to the previous bottom-up models for an r^2 value due to the random noise. This highlights the importance of including variance driven by the predictor variables because it allows the upper tail of the data distribution to be captured. This also suggests there is a limit on the potential to predict large scale patterns of POC flux without the inclusion of σ due to the intrinsic stochasticity always present in POC flux measurements.

3.2. Predictor Dependencies

The effect sizes of SST, Chl-*a* and depth on μ and σ are represented in Figure 3, showing both the overall effect of the predictor and the influence of each singular term. SST and Chl-*a* both positively influence μ with mean effect

10.1029/2026GL123203

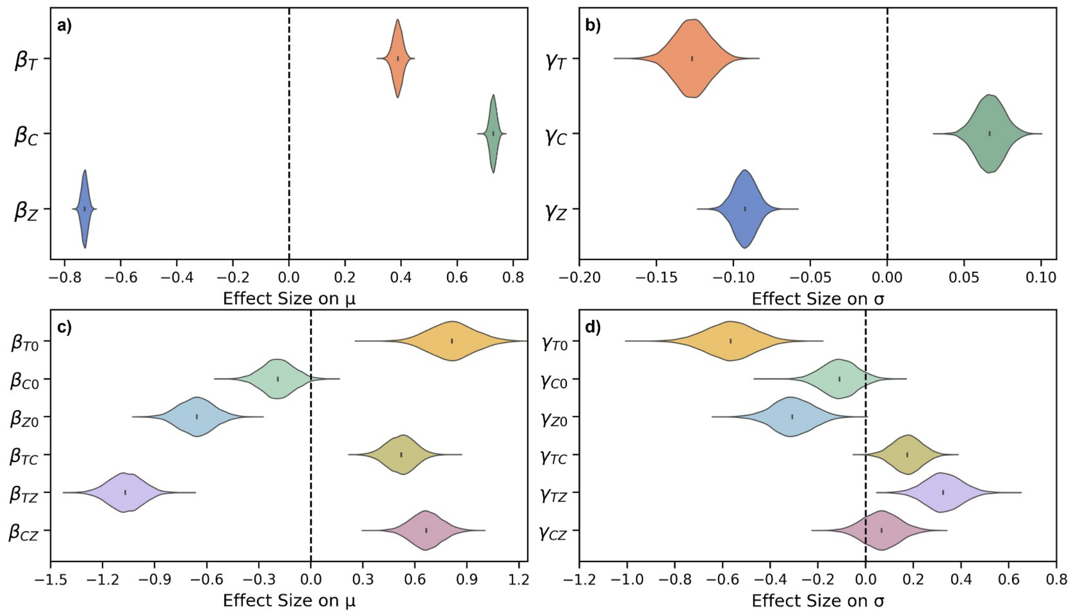

Figure 3. Distributions of the effect size of ln(SST +1.79) (T), ln(Chl-*a*) (C) and ln(depth) (Z) on (a, c) μ, the log-mean, and (b, d) σ, the log-variance. Both (a) and (b) show the summative effect size of each parameter, while (c) and (d) show the individual effect sizes for each parameter and their cross-terms. All effect sizes are normalized through multiplying by the standard deviation of the main parameter. Summative effect sizes are standardized by multiplying by the standard deviation of the overall factor.

sizes of 0.39 (posterior SD 0.016) and 0.73 (posterior SD 0.011) respectively, whereas μ decreases with depth, with a mean effect size of −0.73 (posterior SD 0.011) (Figure 3a). This relationship of depth and Chl-*a* to POC flux is expected: POC flux decreases with depth due to remineralization and high POC flux is generally associated with areas of high NPP so by proxy, high Chl-*a* (Bristow et al., 2017; Laws et al., 2011; Martin et al., 1987). The positive relationship between SST and μ contradicts previous estimates which have found negative correlations between temperature and POC flux, wither warmer regions such as oligotrophic gyres generally having lower export (Henson et al., 2011; Laws et al., 2011). This difference is likely because Chl-*a* is a stronger driver of μ; in our model, regions with high SST would also need high NPP to have the highest levels of export.

The inclusion of σ within the model is also likely to play a role in the relationships SST and Chl-*a* have to patterns in μ. SST has a negative effect on σ with a mean effect size of −0.12 (posterior SD 0.011) suggesting variance decreases with increasing temperature (Figure 3b). Higher latitudes have a higher likelihood of pulse events of POC flux (Cael et al., 2021; Ducklow et al., 2015; Williams et al., 2025). Therefore, the difference in the relationship of SST to the background flux in comparison to previous estimates may also be due to the episodic nature of POC flux in cooler regions. The effect sizes of depth and Chl-*a* on σ are smaller, with Chl-*a* having close to no effect with a mean of 0.067 (posterior SD 9.0×10^{-3}) suggesting little variation in flux with changing Chl-*a* (Figure 3b). Depth has a mean effect size of −0.093 on σ (posterior SD 7.2×10^{-3}) (Figure 3b). This is likely because the absolute magnitude of flux also decreases with β_Z, therefore variability will be reduced. The extremely small posterior standard deviation values for all overall effect sizes on both σ and μ suggests a high degree of confidence in the parameter estimates.

3.3. Global Distributions and Observed Patterns

3.3.1. POC Flux Estimates

We find strong latitudinal patterns in POC flux, where μ is high at the equator and low at the poles with the opposite for σ (Figures 4a and 4b). This suggests that the background flux at the equator is high and is influenced by low episodicity, and *vice-versa* in polar regions. It is important to note that the values in polar regions in these maps are not representative of an annual climatology and instead show the average of the months where data is present due to the reduced availability of satellite data at high latitudes (Figure S5 in Supporting Information S1).

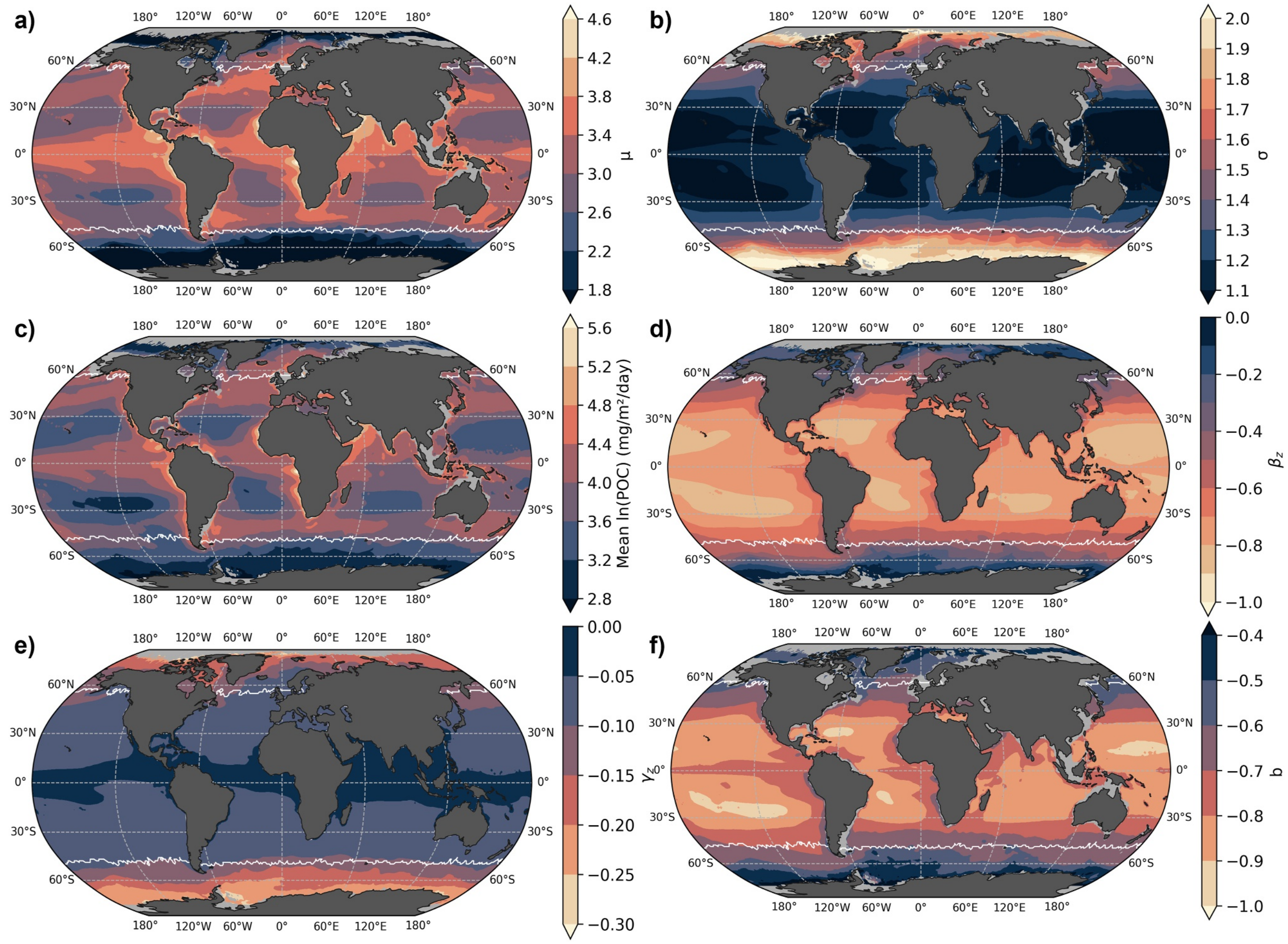

Figure 4. Climatological maps of POC flux. (a) μ, the log-median of POC flux, (b) σ, the log-variance of POC flux, (c) Mean POC flux, (d) β_z, the change in log-median with depth, (e) γ_z, the change in log-variance with depth and (f) a global estimation of Martin's b parameter describing flux attenuation with depth. Maps (a–c) show the flux on a log-scale. Note that poleward of the white line in all maps fewer than 12 months of satellite data are available. A map showing the number of months of data included in the mean is shown in Figure S5 in Supporting Information S1.

The latitudinal patterns of σ reflect the variation in pulse events, not seasonal variation; σ is a representation of variability of POC flux on the scale of individual measurements, which is distinct from variation due to the seasonal cycle. In other words, large σ at high latitudes is because pulse events of POC fluxes are negatively related to SST, not because higher latitudes have larger seasonal variability. These spatial patterns also persist seasonally (Figures S6–S8 in Supporting Information S1). High stochasticity in POC flux at higher latitudes could be explained by a tendency for these regions to experience "bloom and bust" cycles resulting in pulse events (Cael et al., 2021; Ducklow et al., 2015; Williams et al., 2025).

The predicted distribution of mean POC flux follows a mix of the pattern in μ and σ with the lowest export in the gyres and the highest in coastal and mid latitudes (Figure 4c). The globally integrated annual flux at 100 m depth is 6.1 ± 0.17 GtC yr^{-1}. This estimate is highly comparable to recent estimates at 100 m including top-down of 6.7 ±0.2 GtC yr^{-1} and 6.4 GtC yr^{-1} (IQR 6.0-6.7) and a composite of biogeochemical model estimates of 6.1 ± 1.17 GtC yr^{-1} (DeVries & Weber, 2017; Doney et al., 2024; Nowicki et al., 2022). This further supports that by including variance within our statistical model, we can capture a global POC flux estimate that explicitly resolves episodicity. In comparison to other previous bottom-up estimates of global POC flux, our estimate is slightly higher (Clements et al., 2023; Henson et al., 2011; Siegel et al., 2014). However, it is likely our estimate would be higher if calculated at a variable euphotic depth instead of 100 m (Buesseler et al., 2020).

The global integrated POC flux when σ is not included is 3.0 ± 0.074 GtC yr^{-1} (Figure 4b). This demonstrates how our inclusion of variance driven by high-flux, episodic pulse events generates a substantially larger estimate. In fact, the inclusion of episodicity accounts for 52% of the estimated global POC flux. This difference is similar to the proposed impact other export pathways have on the total POC flux (~ 40%) and could be an equally likely explanation for discrepancies in supply of POC and metabolic demand in mesopelagic carbon budgets (Boyd et al., 2019; Burd et al., 2010; Siegel et al., 2023).

Mean annual POC flux follows global spatial patterns similar to those of previous studies, generally reflecting areas of high NPP (e.g., DeVries & Weber, 2017; Henson et al., 2011; Nowicki et al., 2022; Siegel et al., 2014; Wang et al., 2023) (Figure 4c). However, our results differ from previous approaches which estimate low export at high latitudes, although this could be due to poor ocean color satellite coverage in these regions (e.g., Clements et al., 2023; Henson et al., 2011; Siegel et al., 2014). Our model allows higher POC flux to be captured at high latitudes through the addition of σ.

3.3.2. Attenuation Patterns

The spatial pattern of b suggests higher attenuation rates at the equator and oceanic gyres and low pole-ward (Figure 4f), similar to previous research (DeVries & Weber, 2017; Marsay et al., 2015; Weber et al., 2016). This pattern is consistent with increased metabolic rates at higher temperatures, which would enhance remineralization rates and therefore drive greater flux attenuation (DeVries & Weber, 2017).

These patterns can be partially broken down into the patterns of β_Z and γ_Z, and, although not mathematically identical, show the rate change in log-median flux and variance with depth (Figures 4d and 4e). The patterns of β_z are driven by a negative relationship with SST $\left(\beta_{TZ}\right)$ and a positive with Chl-a $\left(\beta_{CZ}\right)$, suggesting higher attenuation rates at lower Chl-a and higher temperatures (Figure 3c). The latitudinal patterns in β_Z are especially driven by the strong contribution of SST through the cross-term β_{TZ} to β_Z (Figure 4d). These relationships may appear because the colder temperatures inhibit remineralizing bacteria and there are more complex planktonic communities at higher latitudes (DeVries & Weber, 2017).

The global distribution of γ_Z suggests higher variability in the relationship between upper ocean and interior POC fluxes at high latitudes, with little to no variability at the equator (Figure 4e). This distribution is driven mainly by γ_{TZ} (Figure 3d), suggesting higher variation in attenuation rates with SST in the episodic flux. Considering previously proposed driving factors of attenuation, this is plausible with plankton community and therefore particle size at high latitudes and lower temperatures being more variable which will result in the episodic attenuation patterns (Guidi et al., 2009; Weber et al., 2016). This also coincides with research by Rufas et al. (2025), which suggests that latitudinal patterns of transfer efficiency may be masked by the variability present in measurements; we are able to capture this within γ_Z. This is interesting when considering the patterns of γ_Z which is lowest at low latitudes, suggesting less variability in the remineralization-depth relationship of β_Z (Figure 4e). The higher variability in attenuation at the poles could also explain why previous global representations of b disagree, where the empirical relationships and smaller data sets do not allow the capture of polar episodicity.

3.4. Limitations and Future Approaches

This paper only focuses on quantifying the gravitational pump so we do not explicitly include variables for the influence of physical or active pathways or on POC flux (Boyd et al., 2019). Although this approach suggests that including pulse events in POC flux estimates to be of similar importance to accounting for other export pathways, this technique could, in principle, be extended to estimate the magnitude of these additional pathways. However, to achieve this, a large reliable database of active and physical pump contributions would be needed. It is also important to note that the predictors we use here, Chl-a and SST, are only proxies for the complex processes involved in POC flux generation and attenuation, for example, fragmentation, aggregation and community structure. Although these predictors work well in capturing the episodicity of the BCP, it is still unclear what the true drivers behind large pulse events are. Future work could combine this methodology and results with a mechanistic process model and other carbon fluxes to explain drivers and patterns in both mean and episodicity of flux.

This methodology also intrinsically includes measurement noise as part of the episodicity, with sediment traps both under and oversampling as a result of measurement depth, design and external environmental factors (Bisson et al., 2018, and references therein). This could influence σ as a result, but separating environmental stochasticity from measurement error and therefore quantifying the latter's influence on σ is not possible from the available measurements.

4. Summary and Conclusions

Here we apply a Bayesian hierarchical approach to estimate global POC flux that incorporates the episodicity in POC flux data as a function of potential drivers (SST, Chl-*a* and depth). The novelty of our method lies in including the effect of episodic pulse events on total POC flux via modeling the variance of POC flux distribution and results in a global export estimate of 6.1 GtC yr^{-1} at 100 m. By explicitly accounting for stochasticity in our statistical model, the total POC flux estimate and spatial pattern is similar to previous estimates, including top-down models where variability introduced by pulse events is intrinsically included. Overall, accounting for the variance of POC flux is an important factor, contributing 52% of the global estimation. The distribution of POC flux was explained by just three variables which are known or readily observable from satellites, allowing for high spatio-temporal coverage. Pulse events that are otherwise missed when using climatologies were captured in relationships for both the magnitude of POC flux and its variance. Patterns of attenuation can also be mapped, with the highest attenuation rates where there are higher temperatures and low primary production. Attenuation is lower at the poles, but with notably more episodicity, suggesting attenuation will fluctuate at the poles with pulse events. Going forward, future estimates that try to capture the total magnitude of the BCP should consider stochasticity within the measurements, with focus on the conditions that result in pulse events.

Conflict of Interest

The authors declare no conflicts of interest relevant to this study.

Availability Statement

The OC-CCI data used in this paper is available at https://www.oceancolour.org The SST data used in this paper is available at https://doi.org/10.5065/r33v-sv91 The POC flux database used in this paper is to be available through publication Ramondenc et al. (2026). A subset of this data used for this research is available here at: https://github.com/sramondenc/Carbon-flux-databaseEdwards-et-alv2026-mars (Ramondenc, 2026). The code for the Hierarchical model and analyses can be found at https://doi.org/10.5281/zenodo.20793937 (Edwards, 2026). The statistical output can also be found at https://doi.org/10.5281/zenodo.20793937 (Edwards, 2026).

Acknowledgments

PE, LG, SH, SR, and BC were supported by Schmidt Sciences (project: CALIPSO). PE was also supported by the INSPIRE DTP (NE/S007210/1). GLB was supported by the Simons Foundation (SFI-LS-ECIAMEE-00012823). We would like to thank ESA, collaborators and the authors of the OC-CCI project for the freely available use of the OC-CCI data products. We would also like to thank NOAA alongside the authors, collaborators and the National Center for Atmospheric Research Staff for freely available use of the Merged Hadley-NOAA/OI Sea Surface Temperature data set.

References

Bisson, K., Siegel, D., DeVries, T., Cael, B., & Buesseler, K. (2018). How data set characteristics influence ocean carbon export models. *Global Biogeochemical Cycles*, *32*(9), 1312–1328. https://doi.org/10.1029/2018GB005934

Boyd, P. W., Claustre, H., Levy, M., Siegel, D. A., & Weber, T. (2019). Multi-faceted particle pumps drive carbon sequestration in the ocean. *Nature*, *568*(7752), 327–335. https://doi.org/10.1038/s41586-019-1098-2

Bressac, M., Laurenceau-Cornec, E., Kennedy, F., Santoro, A., Paul, N., Briggs, N., et al. (2024). Decoding drivers of carbon flux attenuation in the oceanic biological pump. *Nature*, *633*(8030), 587–593. https://doi.org/10.1038/s41586-024-07850-x

Bristow, L. A., Mohr, W., Ahmerkamp, S., & Kuypers, M. M. M. (2017). Nutrients that limit growth in the ocean. *Current Biology*, *27*(11), R474–R478. https://doi.org/10.1016/j.cub.2017.03.030

Britten, G. L., Mohajerani, Y., Primeau, L., Aydin, M., Garcia, C., Wang, W.-L., et al. (2021). Evaluating the benefits of Bayesian hierarchical methods for analyzing heterogeneous environmental datasets: A case study of marine organic carbon fluxes. *Frontiers in Environmental Science*, *9*, 491636. https://doi.org/10.3389/fenvs.2021.491636

Buesseler, K. O., Boyd, P. W., Black, E. E., & Siegel, D. A. (2020). Metrics that matter for assessing the ocean biological carbon pump. *Proceedings of the National Academy of Sciences*, *117*(18), 9679–9687. https://doi.org/10.1073/pnas.1918114117

Burd, A. B., Hansell, D. A., Steinberg, D. K., Anderson, T. R., Arístegui, J., Baltar, F., et al. (2010). Assessing the apparent imbalance between geochemical and biochemical indicators of meso- and bathypelagic biological activity: What the @$#! is wrong with present calculations of carbon budgets? *Deep Sea Research Part II: Topical Studies in Oceanography*, *57*(16), 1557–1571. https://doi.org/10.1016/j.dsr2.2010.02.022

Cael, B. B., Bisson, K., Conte, M., Duret, M. T., Follett, C. L., Henson, S. A., et al. (2021). Open ocean particle flux variability from surface to seafloor. *Geophysical Research Letters*, *48*(9), e2021GL092895. https://doi.org/10.1029/2021GL092895

Cael, B. B., Bisson, K., & Follett, C. L. (2018). Can rates of ocean primary production and biological carbon export be related through their probability distributions? *Global Biogeochemical Cycles*, *32*(6), 954–970. https://doi.org/10.1029/2017GB005797

Carpenter, B., Gelman, A., Hoffman, M. D., Lee, D., Goodrich, B., Betancourt, M., et al. (2017). Stan: A probabilistic programming language. *Journal of Statistical Software*, *76*, 1–32. https://doi.org/10.18637/jss.v076.i01

Clements, D. J., Yang, S., Weber, T., McDonnell, A. M. P., Kiko, R., Stemmann, L., & Bianchi, D. (2023). New estimate of organic carbon export from optical measurements reveals the role of particle size distribution and export horizon. *Global Biogeochemical Cycles*, *37*(3), e2022GB007633. https://doi.org/10.1029/2022GB007633

DeVries, T., & Weber, T. (2017). The export and fate of organic matter in the ocean: New constraints from combining satellite and oceanographic tracer observations. *Global Biogeochemical Cycles*, *31*(3), 535–555. https://doi.org/10.1002/2016GB005551

Doney, S. C., Mitchell, K. A., Henson, S. A., Cavan, E., DeVries, T., Gruber, N., et al. (2024). Observational and numerical modeling constraints on the global ocean biological carbon pump. *Global Biogeochemical Cycles*, *38*(7), e2024GB008156. https://doi.org/10.1029/2024GB008156

Ducklow, H. W., Wilson, S. E., Post, A. F., Stammerjohn, S. E., Erickson, M., Lee, S., et al. (2015). Particle flux on the continental shelf in the Amundsen Sea Polynya and western Antarctic Peninsula. *Elementa*, *3*, 000046. https://doi.org/10.12952/journal.elementa.000046

Dunne, J. P., Sarmiento, J. L., & Gnanadesikan, A. (2007). A synthesis of global particle export from the surface ocean and cycling through the ocean interior and on the seafloor. *Global Biogeochemical Cycles*, *21*(4), 2006GB002907. https://doi.org/10.1029/2006GB002907

Edwards, P. (2026). Sample code and dataset for capturing the global variability of marine particulate organic carbon flux: A hierarchical Bayesian approach (v1.1). *Zenodo*. https://doi.org/10.5281/zenodo.20793937

Garcia, H. E., Bouchard, C., Cross, S. L., Paver, C. R., Boyer, T. P., Reagan, J. R., et al. (2024). World ocean atlas 2023, volume 4: Dissolved inorganic nutrients (phosphate, nitrate, silicate) [Dataset]. *National Centers for Environmental Information (NCEI), NOAA*. https://doi.org/10.25923/39qw-7j08

Gelman, A., & Rubin, D. B. (1992). Inference from iterative simulation using multiple sequences. *Statistical Science*, *7*(4), 457–472. https://doi.org/10.1214/ss/1177011136

Guidi, L., Legendre, L., Reygondeau, G., Uitz, J., Stemmann, L., & Henson, S. A. (2015). A new look at ocean carbon remineralization for estimating deepwater sequestration. *Global Biogeochemical Cycles*, *29*(7), 1044–1059. https://doi.org/10.1002/2014GB005063

Guidi, L., Stemmann, L., Jackson, G. A., Ibanez, F., Claustre, H., Legendre, L., et al. (2009). Effects of phytoplankton community on production, size, and export of large aggregates: A world-ocean analysis. *Limnology and Oceanography*, *54*(6), 1951–1963. https://doi.org/10.4319/lo.2009.54.6.1951

Henson, S. A., Sanders, R., & Madsen, E. (2012). Global patterns in efficiency of particulate organic carbon export and transfer to the deep ocean. *Global Biogeochemical Cycles*, *26*(1). https://doi.org/10.1029/2011GB004099

Henson, S. A., Sanders, R., Madsen, E., Morris, P. J., Le Moigne, F., & Quartly, G. D. (2011). A reduced estimate of the strength of the ocean's biological carbon pump. *Geophysical Research Letters*, *38*(4). https://doi.org/10.1029/2011GL046735

Hurrell, J. W., Hack, J. J., Shea, D., Caron, J. M., & Rosinski, J. (2008). A new sea surface temperature and sea ice boundary dataset for the community atmosphere model. *Journal of Climate*, *21*(19), 5145–5153. https://doi.org/10.1175/2008JCLI2292.1

Iversen, M. H. (2023). Carbon export in the ocean: A biologist's perspective. *Annual Review of Marine Science*, *15*(1), 357–381. https://doi.org/10.1146/annurev-marine-032122-035153

Lambert, B. (2018). *A student's guide to Bayesian statistics*. SAGE Publications.

Laws, E. A., D'Sa, E., & Naik, P. (2011). Simple equations to estimate ratios of new or export production to total production from satellite-derived estimates of sea surface temperature and primary production. *Limnology and Oceanography: Methods*, *9*(12), 593–601. https://doi.org/10.4319/lom.2011.9.593

Lévy, M., Bopp, L., Karleskind, P., Resplandy, L., Ethe, C., & Pinsard, F. (2013). Physical pathways for carbon transfers between the surface mixed layer and the ocean interior. *Global Biogeochemical Cycles*, *27*(4), 1001–1012. https://doi.org/10.1002/gbc.20092

Marsay, C. M., Sanders, R. J., Henson, S. A., Pabortsava, K., Achterberg, E. P., & Lampitt, R. S. (2015). Attenuation of sinking particulate organic carbon flux through the mesopelagic ocean. *Proceedings of the National Academy of Sciences*, *112*(4), 1089–1094. https://doi.org/10.1073/pnas.1415311112

Martin, J. H., Knauer, G. A., Karl, D. M., & Broenkow, W. W. (1987). VERTEX: Carbon cycling in the northeast Pacific. *Deep-Sea Research, Part A: Oceanographic Research Papers*, *34*(2), 267–285. https://doi.org/10.1016/0198-0149(87)90086-0

Nowicki, M., DeVries, T., & Siegel, D. A. (2022). Quantifying the carbon export and sequestration pathways of the ocean's biological carbon pump. *Global Biogeochemical Cycles*, *36*(3), e2021GB007083. https://doi.org/10.1029/2021GB007083

Ramondenc, S. (2026). Carbon flux database—Specific subset. *Github*. https://github.com/sramondenc/Carbon-flux-databaseEdwards-et-alv2026-mars

Ramondenc, S., Wynn-Edwards, C., Le Quéré, C., Guest, J., Henson, S., Bancel, V., et al. (2026). Global database of particulate organic carbon flux in the ocean: Integration of in situ observation, satellite, and model products. in prep.

Resplandy, L., Lévy, M., & McGillicuddy, D. J., Jr. (2019). Effects of eddy-driven subduction on ocean biological carbon pump. *Global Biogeochemical Cycles*, *33*(8), 1071–1084. https://doi.org/10.1029/2018GB006125

Rufas, A., Khatiwala, S., Bisson, K., Martin, A., & Bouman, H. (2025). Can we constrain geographical variability in the biological carbon pump's transfer efficiency from observations? *Geophysical Research Letters*, *52*(3), e2024GL111203. https://doi.org/10.1029/2024GL111203

Sathyendranath, S., Brewin, R. J., Brockmann, C., Brotas, V., Calton, B., Chuprin, A., et al. (2019). An ocean-colour time series for use in climate studies: The experience of the ocean-colour climate change initiative (OC-CCI). *Sensors*, *19*(19), 4285. https://doi.org/10.3390/s19194285

Sathyendranath, S., Jackson, T., Brockmann, C., Brotas, V., Calton, B., Chuprin, A., et al. (2023). *ESA ocean colour climate change initiative (ocean_colour_cci): Version 6.0, 4km resolution data*. NERC EDS Centre for Environmental Data Analysis. https://doi.org/10.5285/5011D22AAE5A4671B0CBC7D05C56C4F0

Shea, D., Hurrell, J., & Phillips, A. (2024). Merged Hadley-OI sea surface temperature and sea ice concentration data set. *Zenodo*. https://doi.org/10.5065/r33v-sv91

Siegel, D. A., Buesseler, K. O., Doney, S. C., Sailley, S. F., Behrenfeld, M. J., & Boyd, P. W. (2014). Global assessment of ocean carbon export by combining satellite observations and food-web models. *Global Biogeochemical Cycles*, *28*(3), 181–196. https://doi.org/10.1002/2013GB004743

Siegel, D. A., DeVries, T., Cetinić, I., & Bisson, K. M. (2023). Quantifying the ocean's biological pump and its carbon cycle impacts on global scales. *Annual Review of Marine Science*, *15*(1), 329–356. https://doi.org/10.1146/annurev-marine-040722-115226

Smith, K. L., Ruhl, H. A., Huffard, C. L., Messié, M., & Kahru, M. (2018). Episodic organic carbon fluxes from surface ocean to abyssal depths during long-term monitoring in NE Pacific. *Proceedings of the National Academy of Sciences*, *115*(48), 12235–12240. https://doi.org/10.1073/pnas.1814559115

Trudnowska, E., Lacour, L., Ardyna, M., Rogge, A., Irisson, J. O., Waite, A. M., et al. (2021). Marine snow morphology illuminates the evolution of phytoplankton blooms and determines their subsequent vertical export. *Nature Communications*, *12*(1), 2816. https://doi.org/10.1038/s41467-021-22994-4

Volk, T., & Hoffert, M. I. (1985). Ocean carbon pumps: Analysis of relative strengths and efficiencies in ocean-driven atmospheric CO_2 changes. In *The carbon cycle and atmospheric CO_2: Natural variations Archean to present* (Vol. 32, pp. 99–110). https://doi.org/10.1029/GM032p0099

10.1029/2026GL123203

Wang, W.-L., Fu, W., Le Moigne, F. A. C., Letscher, R. T., Liu, Y., Tang, J.-M., & Primeau, F. W. (2023). Biological carbon pump estimate based on multidecadal hydrographic data. *Nature*, *624*(7992), 579–585. https://doi.org/10.1038/s41586-023-06772-4

Weber, T., Cram, J. A., Leung, S. W., DeVries, T., & Deutsch, C. (2016). Deep ocean nutrients imply large latitudinal variation in particle transfer efficiency. *Proceedings of the National Academy of Sciences*, *113*(31), 8606–8611. https://doi.org/10.1073/pnas.1604414113

Williams, J. R., Giering, S. L. C., Baker, C. A., Pabortsava, K., Briggs, N., East, H., et al. (2025). Inefficient transfer of diatoms through the subpolar southern ocean twilight zone. *Nature Geoscience*, *18*(1), 72–77. https://doi.org/10.1038/s41561-024-01602-2